Polarisation-sensitive four-wave mixing and soliton self-frequency shift effect in the highly birefringent photonic crystal fibre*

Yuan Jin-Hui(苑金辉)[a)†], Sang Xin-Zhu(桑新柱)[a)], Yu Chong-Xiu (余重秀)[a)], Xin Xiang-Jun(忻向军)[a)], Li Shu-Guang(李曙光)[b)], Zhou Gui-Yao(周桂耀)[b)], and Hou Lan-Tian(侯蓝田)[b)]

[a)] *Key Laboratory of Information Photonics and Optical Communications, Ministry of Education, Institute of Optical Communication and Optoelectronics, Beijing University of Posts and Telecommunications, Beijing* 100876, *China*
[b)] *Institute of Infrared Optical Fibers and Sensors, College of Information Science and Engineering, Yanshan University, Qinhuangdao* 066004, *China*

(Received 20 September 2009; revised manuscript received 9 December 2009)

By adjusting the polarisation state of the pump at 805 nm parallel to slow (x) and fast (y) axes of the highly birefringent photonic crystal fibre with zero dispersion wavelengths 790 nm and 750 nm, this paper demonstrates the efficient polarisation-sensitive four wave mixing involved in pump, anti-Stokes and Stokes signals and soliton self-frequency shift effects induced by the phase-matching between red-shifted solitons and blue-shifted dispersive waves. If the reduction of coupling efficiency to the circular pump laser mode or other circular fibres due to asymmetry of the core is neglected, more than 98% of the total input power is kept in a single linear polarisation. Controlled dispersion characteristic of the doublet of fundamental guided-modes results in achieving light field strongly confined in principal axes of photonic crystal fibre, and enhancing the corresponding nonlinear-optical process through the remarkable nonlinear birefringence.

Keywords: highly birefringent photonic crystal fibre, four wave mixing, soliton self-frequency shift, phase-matching

PACC: 4281D, 4281F, 4265M, 4265S

1. Introduction

Because of the flexibility in designing optical properties of light, such as nonlinearity, dispersion and birefringence,[1−3] photonic-crystal fibres (PCFs) have opened a new phase and are found many applications in nonlinear optics,[4−6] such as an excess to the carrier-envelop phase,[7] creation of the novel optical coherence tomography,[8] the nonlinear spectrographs,[9] and extension of the application range of femtosecond laser sources to photochemistry and photobiology.[10] The remarkable structure flexibility of PCFs means interesting strategies for the design of fibres with a high modal birefringence.[11,12] One way to achieve the high birefringence is stress-induction, and another way is realised through asymmetric microstructure near the core.[13,14] Besides the linear birefringence, the nonlinear birefringence induced by high power intensity concentrating on principal axes allows efficient polarisation control of nonlinear phenomena including frequency conversion based on phase-matching four-wave mixing (FWM),[15,16] blue-shift dispersive wave[17,18] due to soliton self-frequency shift (SSFS), and supercontinuum generation[19−22] through the combination of different nonlinear effects.

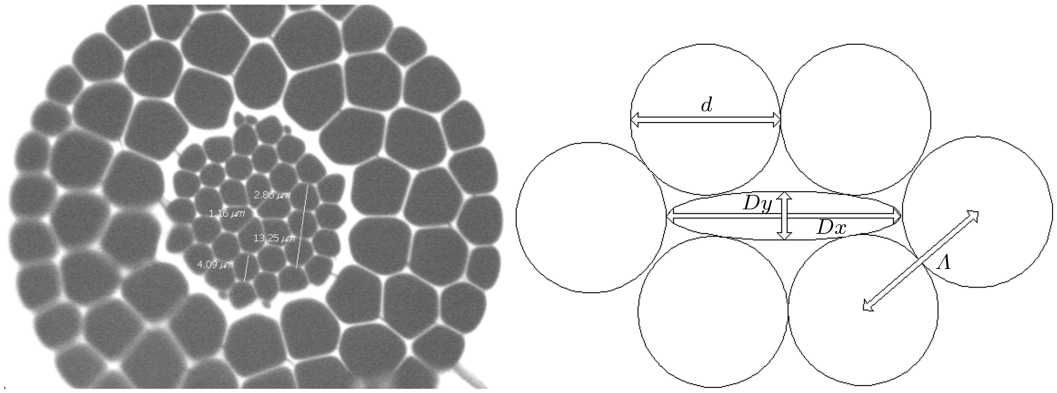
Here, the strong single polarisation along slow (x) and fast (y) axes (98% of the total power in a single linear polarisation) is achieved with the highly birefringent PCF fabricated by improved twice stack-and-draw technique.[23] The highly efficient frequency conversion is based on the efficient polarisation-sensitive FWM, which involves a pump and a Stokes wave at frequency $\omega_{\rm p}$ and $\omega_{\rm S}$, and the generated signal wave at $2\omega_{\rm p}-\omega_{\rm S}$. The corresponding propagation constants of pump $\beta(\omega_{\rm p})$, anti-Stokes $\beta(\omega_{\rm a})$ and Stokes signals $\beta\,(\omega_{\rm S})$ meet the phase-matching condition along x and

*Project partly supported by the National Basic Research Program (Grant Nos. 2010CB327605 and 2010CB328300), National High-Technology Research and Development Program of China (Grant Nos. 2007AA03Z447 and 2009AA01Z220), the National Natural Science Foundation of China (Grant No. 60807022), the Key Grant of Ministry of Education of China (Grant No. 109015) and the Specialized Research Fund for the Doctoral Program of Higher Education of China (Grant No. 20070013001).
†Corresponding author. E-mail: yuanjinhui81@163.com
© 2010 Chinese Physical Society and IOP Publishing Ltd

y axes at $\delta\beta_{\rm FWM} = 2\beta(\omega_{\rm p}) - \beta(\omega_{\rm a}) - \beta(\omega_{\rm S}) = 0$. The SSFS provides a resonant energy exchange between red-shifted solitons with propagation constant $\beta_{\rm s}$ and central wavelength λ_0 and blue-shifted dispersive waves with propagation constant $\beta_{\rm d}$ and central wavelength $\lambda_{\rm d}$.

2. Highly birefringent PCF and experimental setup

The cross-section structure and sketch map of the inner core of PCF used in the experiment are shown in Fig. 1(a) and 1(b). The cladding hole diameter $d = 5.24$ μm, hole pitch $\Lambda = 4.5$ μm. An elliptically deformed core gives rise to form birefringence and the measured parameters are as follows: $Dx = 2.86$ μm and $Dy = 1.16$ μm along the long (x) and short (y) axes, the ratio is 2.47. The reduction of coupling efficiency to the circular pump laser mode or other circular fibres due to asymmetry of the core is neglected. The fibre attenuation was measured to be about 0.015 dB/m at 805 nm using the cut-back technique, and the calculated polarisation beat length at 805 nm is 9.45 mm.



(a) (b)

Fig. 1. (a) The cross-section structure of highly birefringent PCF; (b) the sketch map corresponding to the inner core region.

Multi-pole method has been used to analyse the properties of fundamental mode in PCF.[24] The group-velocity dispersion D for the doublet of fundamental modes passes through zero at different wavelengths corresponding to 790 nm and 750 nm along the x and y axes of the fibre core as shown in Fig. 2(a), respectively, and the frequency-shifted processes originate from SSFS and phase-matched FWM effects. The material dispersion is analysed from Sellmeyer equation. The elliptical and near-circular shapes of output mode field along x and y axes are shown in inserts 1 and 2 of Fig. 2(a). For both modes, the input laser field with central wavelength at 805 nm is falling within the anomalous dispersion region approaching to the zero dispersion wavelengths of two polarisation fundamental mode, and the phase-matching FWM $2\omega_{\rm p} = \omega_{\rm S} + \omega_{\rm a}$ is prone to occur. The doublet modes polarised along the x and y axes have different propagation constants $\beta_x = \beta_0 + \delta\beta_x$ and $\beta_y = \beta_0 + \delta\beta_y$, where β_0 is the propagation constant of the doublet of degenerate fundamental modes in the fibres with a circular core, $\delta\beta_x = 2\beta_x(\omega_{\rm p}) - \beta_x(\omega_{\rm a}) - \beta_x(\omega_{\rm S})$ and $\delta\beta_y = 2\beta_y(\omega_{\rm p}) - \beta_y(\omega_{\rm a}) - \beta_y(\omega_{\rm S})$ are the birefringence-induced corrections to the propagation constant for the modes polarised along the long and short axes of the ellipse core, $\beta_x(\omega_{\rm p})$, $\beta_x(\omega_{\rm a})$, $\beta_x(\omega_{\rm S})$, $\beta_y(\omega_{\rm p})$, $\beta_y(\omega_{\rm a})$, and $\beta_y(\omega_{\rm S})$ are the propagation constants of pump, anti-Stokes, and Stokes signal polarised along the x and y axes in core region, respectively. Moreover, the mutual influence of birefringence on phase-matching can be neglected due to $L >> L_{\rm b}$, where L (45 cm) is the fibre length and $L_{\rm b}$ (9.45 mm) is the polarisation beat length. Figure 2(b) shows the phase-matching curves of FWM with pump polarised along the x and y axes. For the doublet of fundamental modes, we can see that the amplitude of phase-mismatching curve of slow axis mode is smaller than that of fast axis mode due to less deviation of pump wavelength from the zero-dispersion wavelength. The phase-matching condition $\delta\beta_x = 0$ and

$\delta\beta_y = 0$ are met with pump falling at 805 nm, giving rise to remarkable Stokes fields at 2300 nm and 1300 nm (along x axis), at 2100 nm and 1000 nm (along y axis). The corresponding anti-Stokes fields are generated at 560 nm and 465 nm (along x axis), at 600 nm and 455 nm (along y axis). The SSFS and blue-shifted dispersive frequency components take place due to the input laser field falling within the anomalous dispersion region, and the phase-matching conditions $\delta\beta_{Sx} = \beta_{Sx}(\lambda_0) - \beta_{dx}(\lambda_\mathrm{d}) = 0$ and $\delta\beta_{Sy} = \beta_{Sy}(\lambda_0) - \beta_{dy}(\lambda_\mathrm{d}) = 0$ along the slow and fast axis are met. As illustrated in Fig. 2(c), the multiply soliton shift toward longer wavelengths within the ranges from 1160 to 1220 nm along the slow axis and 1260 to 1320 nm along fast axis generated by 805 nm pump, can generate phase-matching dispersive waves in the 480 to 420 nm wavelength range.

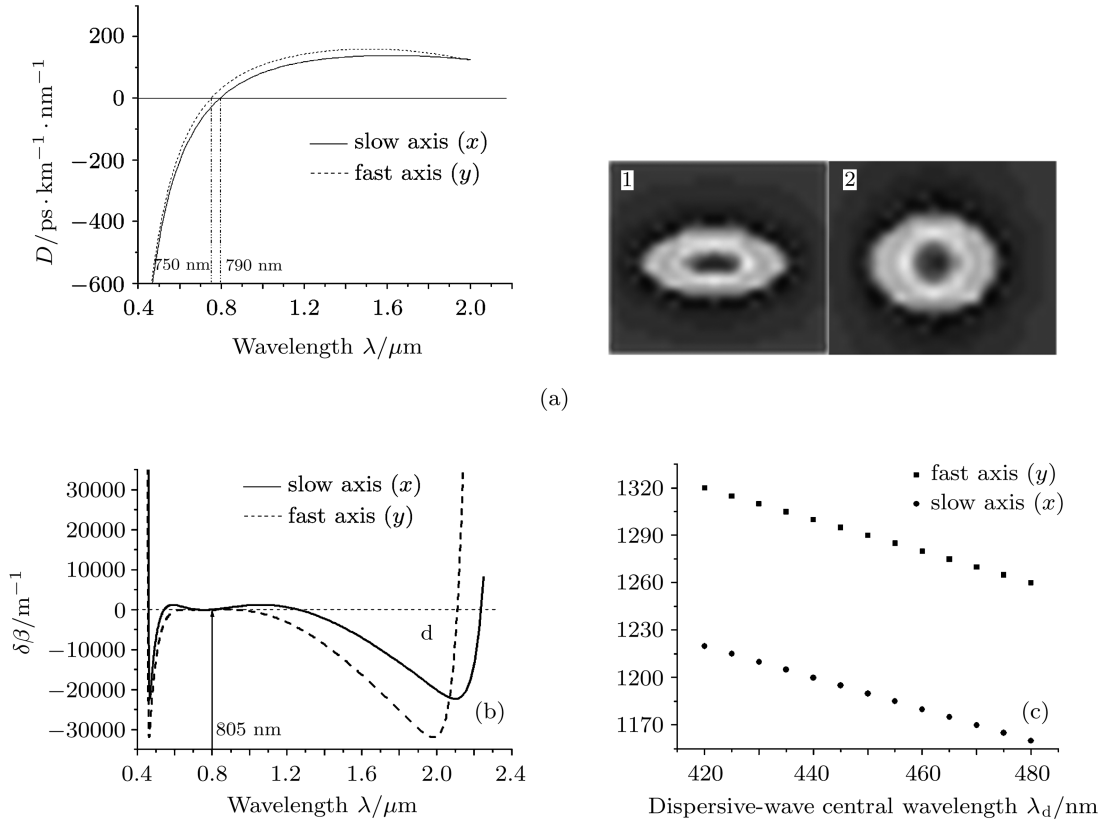


Fig. 2. (a) Group-velocity dispersion D calculated as a function of radiation wavelength for the doublet modes of the fundamental mode of the PCF, the vertical dash line indicates the zero dispersion wavelength along the slow axis (solid line) and fast (dash line) axis; (b) the phase-mismatching in the fundamental doublet modes of PCF along slow axis (solid line) and fast (dash line) axis as a function of radiation wavelength, the vertical dash arrow indicates the input pump wavelength; (c) the phase-matching between the red-shifted soliton and blue-shifted dispersive wave along the slow axis (solid circular dot) and fast axis (solid quadrate dot). Inserts 1 and 2 in Fig. 2(a) show the output near-fields with polarisation direction of pump along slow and fast axes.

The experimental setup configuration is shown in Fig. 3. The pump laser is a mode-locked Ti: sapphire laser with central wavelength 820 nm, emitting a 150 fs pulse train at the repetition rate of 76 MHz. The average input power is 240 mW, and an optical isolator served to protect the laser oscillator from radiation backreflected from the focusing optics and the fibre. A polariser was used to purify the input polarisation, and a rotating half-wave plate was put between the polariser and the fibre input end to adjust the input polarisation. A 40× anti-reflection coated aspheric singlet lens was used to couple laser radiation into the PCF with a length of 45 cm. The input coupling efficiency was as high as 65%. The CCD1 and CCD2 are used to watch the coupling state of input light and output mode fields, and the optical spectrum analyser (OSA) with resolution of 0.1 nm is used to observe the output spectrum.

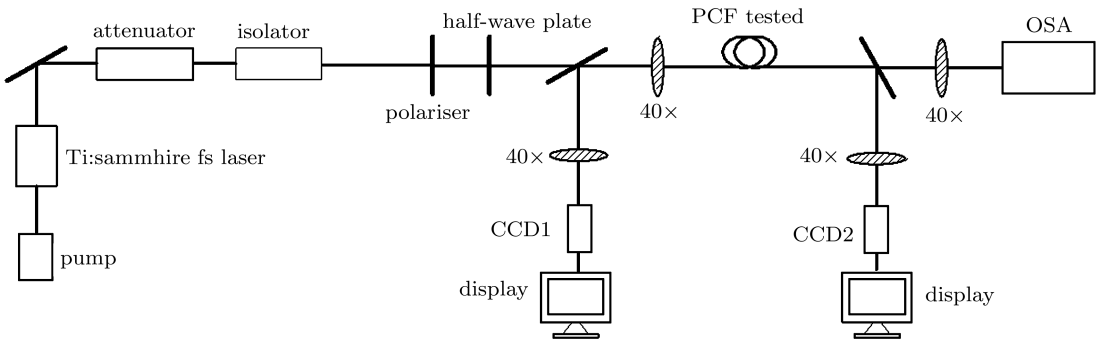


Fig. 3. The configuration of the experimental setup.

3. Experimental results and discussion

The polarisation-sensitive FWM and SSFS processes are carried out with polarisation control of the input field using the polariser and half-wave plate, and the pump wavelength is adjusted to approach at the zero dispersion wavelengths along the slow (x) and fast (y) axis. Figures 4(a) and 4(b) show the output spectral features and near-fields of the birefringent PCF with the input beam aligning along the slow and fast axes and the laser field being coupled into the doublet of fundamental modes.

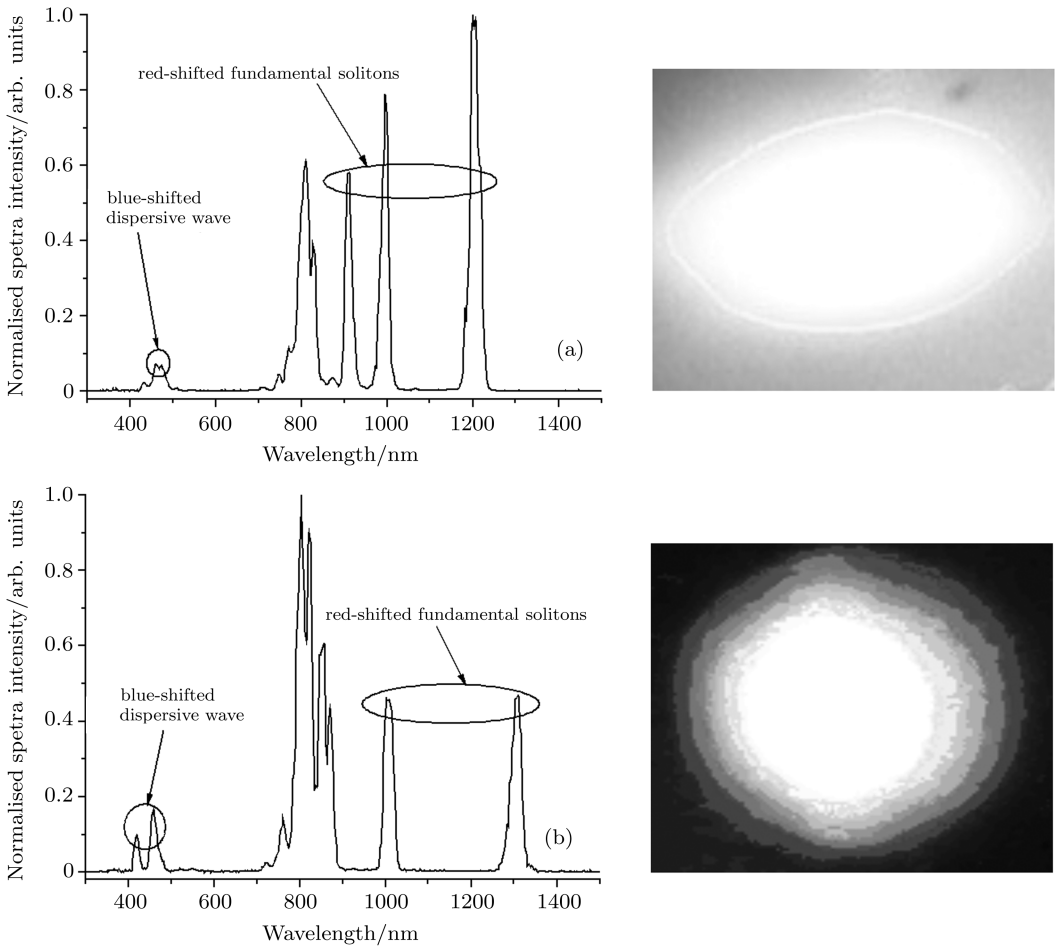


Fig. 4. The output spectrum of highly birefringent PCF with the input pump field polarising along (a) slow (x) and (b) fast (y) axes. Inserts show the corresponding elliptical and circular output near fields.

For the doublet of fundamental modes, the frequency components near the zero-dispersion wavelength of the PCF serve as a pump for phase-matched FWM. These phase-matched FWM processes, which involve both frequency-degenerate and non-degenerate pump photos, occur constantly along the two principal axes, deplete the energy around zero dispersion wavelengths, and transfer the radiation energy to the normal and anomalous dispersion regions. Moreover, because the input laser field lies in the region of anomalous dispersion, it is coupled into solitons due to the combination effect of group velocity dispersion and self-phase modulation. These solitons experience a continuous red-shift induced by the intrapulse Raman scattering as they propagate along the fibre. This process is the Raman-type amplification of the long wavelength part of the pulse spectrum at the expense of the depletion of its short wavelength wing. At the same time, the phase-matching between solitons and dispersive waves are achieved, and the intense blue-shift emissions with the central wavelengths lying in Cherenkov radiation region are generated.[25]

There are three peaks at wavelengths near 910 nm, 1000 nm, and 1210 nm, as shown in Fig. 4(a), and these correspond to the fundamental soliton pulses generated by the fission of the pump pulse,[26] the changing range of the peak position of the fundamental soliton pulse at the longest wavelength is about 300 nm. The peak near 465 nm is a dispersive wave emitted by the fundamental soliton pulse. Correspondingly, in Fig. 4(b), two fundamental soliton pulses with peaks emerging near 1010 nm and 1300 nm are shown, the changing range of peak position is about 290 nm, and two dispersive waves near 465 nm and 435 nm are observed. The peak intensities of three fundamental soliton pulses in Fig. 4(a) are much higher than the ones in Figs. 4(b), and the main reason is from the high polarisation of input pump pulse along principal axis, which lead to much higher polarisation extinction ratio. Although the red-shifted range of fundamental soliton with 300 nm in Fig. 4(a) is nearly equivalent to the one with 290 nm in Fig. 4(b), the longest wavelengths correspond to 1210 nm and 1300 nm, respectively. The possible reasons are considered as follows. On the one hand, there are existing larger pump wavelength deviations from zero dispersion wavelengths along y axis than x axis, which enhance the energy intensity coupled into solitons along y direction. On the other hand, the input pump pulse may be coupled into higher-order modes, and induces more complicated soliton dynamic process, giving rise to a continuous red-shifted radiation.

Moreover, the transmission loss of fabricated PCF can achieve up to tens of dB/m at longer wavelengths because of practical restrictions of technology, it is possible that the energy of these Stokes components at longer wavelengths is depleted at the output of fibre. The corresponding Stokes components at the phase-matching wavelengths of 2100 nm and 2300 nm are not shown in the output spectrum because of beyond the measurement range of OSA (400 to 1700 nm), and they are likely to be completely depleted as a result of possible hundreds of dB/m transmission loss. In inserts of Figs. 4(a) and 4(b), the output mode fields show elliptical and circular shapes, which are consistent with the simulation result as shown in inserts 1 and 2 of Fig. 2(a), and the main reason is considered to be the intensity-induced nonlinear birefringence. The polarisation extinction ratio (PER)[27,28] is defined as the power ratio between p_s and p_f, where p_s and p_f are the measured power with the output polariser's axis along the slow (x) and fast (y) axes. Because of higher birefringence, the measured output PER was $p_s/p_f = 80$ and $p_f/p_s = 30$ when the input polarisation was along the slow and fast axes (98.75% and 96.7% single polarisation), meaning well linearly polarised characteristics for the output spectral components. The total indices $n'_x = n_x + n_2 p_0/A_{\mathrm{eff}\,x}$, $n'_y = n_y + n_2 p_0/A_{\mathrm{eff}\,y}$, where n_x, n_y ($n_x > n_y$) are the linear indices along x and y axes, where n_2 is the nonlinear index of silica material, p_0 is the input average power, and $A_{\mathrm{eff}\,x}$, $A_{\mathrm{eff}\,y}$ are the effective mode field areas along x and y axes. When the input polarisation is along the slow (x) axis, $n'_x > n_x$ and $n'_y \approx n_y$ are satisfied and the nonlinear birefringence enhances the linear birefringence with increased $\Delta n = n'_x - n'_y$. On the contrary, when the input polarisation is along the fast (y) axis, $n'_y > n_y$ and $n'_x \approx n_x$ are satisfied and the nonlinear birefringence can result in the total cancellation of linear birefringence with decreased $\Delta n = n'_x - n'_y$.

4. Conclusions

In summary, the polarisation-sensitive FWM and SSFS processes have been demonstrated with the highly birefringent PCF by adjusting the polarisation states of input field along the slow and fast axis. Controlled dispersion of the doublet of fundamental guided-modes results in achievement of the input laser

field falling within the anomalous dispersion region, and the phase-matching conditions are met. The light field strongly confined in slow (x) and fast (y) axes in the core region enhances the corresponding nonlinear-optical process through the remarkable nonlinear birefringence, and this is confirmed by the observation of the output spectral features and near-fields in experiment. Our further works are primarily refered to generating polarisation-sensitive supercontinuum with wide and flattened bandwidth through this phase-matching FWM and SSFS using much longer fibres, providing efficient polarisation-adjustable multi-channel light source for the communication system based on radio over fibre.

References

[1] Ranka J K, Windeler R S and Stentz A J 2000 *Opt. Lett.* **25** 796

[2] Birks T A, Mogilevstev D, Knight J C and Russell P S J 1999 *IEEE Photon. Technol. Lett.* **11** 674

[3] Kano P, Barker D and Brio M 2008 *J. Phys.* D: *Appl. Phys.* **41** 185106

[4] Akimov D A, Serebryannikov E E, Zheltikov A M, Schmitt M, Maksimenka R, Kiefer W, Dukel'skii K V, Shevandin V S and Kondrat'ev Yu N 2003 *Opt. Lett.* **28** 1948

[5] Yan F P, Tong Z, Wei H, Pei L, Ning T G, Fu Y J, Zheng K, Wang L, Li Y F, Gong T R and Jian S S 2007 *Chin. Phys.* **16** 1700

[6] Yan F P, Mao X Q, Wang L, Fu Y J, Wei H, Zheng K, Gong T R, Liu P, Tao P L and Jian S S 2009 *Acta Phys. Sin.* **58** 6296 (in Chinese)

[7] Jones D J, Diddams S A, Ranka J K, Stentz A, Windeler R S, Hall J L and Cundiff S T 2000 *Science* **288** 635

[8] Hartl I, Li X D, Chudoba C, Rhanta R K, Ko T H, Fujimoto J G, Ranka J K and Windeler R S 2001 *Opt. Lett.* **26** 608

[9] Paulsen H N, Hilligsøe K M, Thøgersen J, Keiding S R and Larsen J J 2003 *Opt. Lett.* **28** 1123

[10] Konorov S O and Zheltikov A M 2003 *Opt. Express* **11** 2440

[11] Hansen T P, Broeng J, Libori S E B, Knudsen E, Bjarklev A, Jensen J R and Simonsen H 2001 *IEEE Photon. Technol. Lett.* **13** 588

[12] Woliński T R, Ertman S, Czapla A, Lesiak P, Nowecka K and Domański A W 2007 *Meas. Sci. Technol.* **18** 3061

[13] Apolonski Povazay B, Unterhuber A, Drexler W, Wadsworth W J, Knight J C and Russell P S J 2002 *J. Opt. Soc. Am.* B **19** 2165

[14] Yue Y, Kai G Y, Wang Z, Li Y, Zhang C S, Lu Y F, Sun T T, Jin L, Liu J G, Liu Y G, Yuan S Z and Dong X Y 2006 *Opt. Commun.* **268** 46

[15] Hu M L, Wang C Y, Li Y F, Chai L and Zheltikov A M 2005 *Opt. Express* **13** 5947

[16] Hu M L, Wang C Y, Li Y F, Wang Z, Chai L and Zheltikov A M 2005 *IEEE Photon. Technol. Lett.* **17** 630

[17] Hu M L, Wang C Y, Chai L and Zheltikov A M 2004 *Opt. Express* **12** 1932

[18] Lægsgaard J 2007 *J. Opt.* A: *Pure Appl. Opt.* **11** 1105

[19] Lehtonen M, Genty G, Ludvigsen H and Kaivola M 2003 *Appl. Phys. Lett.* **82** 2197

[20] Liu W H, Song X Z, Wang Y S, Liu H J, Zhao W, Liu X M, Peng Q J and Xu Z Y 2008 *Acta Phys. Sin.* **57** 917 (in Chinese)

[21] Chen Y Z, Li Y Z, Qu G and Xu W C 2006 *Acta Phys. Sin.* **55** 717 (in Chinese)

[22] Liu W H, Wang Y S, Liu H J, Duan Z L, Zhao W, Li Y F, Peng Q J and Xu Z Y 2006 *Acta Phys. Sin.* **55** 1815 (in Chinese)

[23] Zhou G Y, Hou Z Y and Hou L T 2006 *Appl. Opt.* **45** 4433

[24] White T P, Kuhlmey B T, McPhedran R C, Maystre D, Renversez G, de Sterke C M and Botten L C 2002 *J. Opt. Soc. Am.* B **19** 2322

[25] Hu M L, Wang C Y, Song Y J, Li Y F, Chai L, Serebryannikov E E and Zheltikov A M 2006 *Opt. Express* **14** 1189

[26] Karasawa N, Tada K and Ohmori H 2007 *IEEE Photon. Technol. Lett.* **19** 1292

[27] Cherif R, Zghal M, Tartara L and Degiorgio V 2008 *Opt. Express* **16** 2147

[28] Prodan L, Hagen R, Gross P, Arts R, Beigang R, Fallnich C, Schirmacher A, Kuipers L and Boller K J 2008 *J. Phys.* D: *Appl. Phys.* **41** 135105